Sol-gel synthesis and micro-Raman characterization of ε-Fe$_2$O$_3$ micro- and nanoparticles

J. López-Sánchez*[†,¤], A. Serrano[†,Ø], A. Del Campo[Ø], M. Abuín[†,◊], O. Rodríguez de la Fuente[†,¤], N. Carmona[†,¤]

† Departamento de Física de Materiales, Universidad Complutense de Madrid, 28040 Madrid

¤ Unidad Asociada IQFR(CSIC)-UCM, 28040 Madrid

Ø Instituto de Cerámica y Vidrio, CSIC, 28049 Madrid

◊CEI Campus Moncloa, UCM-UPM, 28040 Madrid

* Corresponding author: jesus.lopez@ucm.es

Macroscopic aspect of the samples

The samples show two different types of regions (see Figure S1A). In the first one, patches (around tens of microns) are distributed throughout the sample surface. Most probably, these big patches are points of nucleation of amorphous silicon oxide. This assumption has been checked by X-Ray Diffraction (XRD) patterns, which show a broad band around $2\theta = 20°$, corresponding to amorphous silicon oxide matrix (not shown here). Upon them, smaller iron oxide particles can be observed, emerging from the surface and ranging from hundreds of nanometers to about one micrometer. These smaller particles can be also observed surrounding the large patches and spreading out around the whole sample (see Figure S1B).
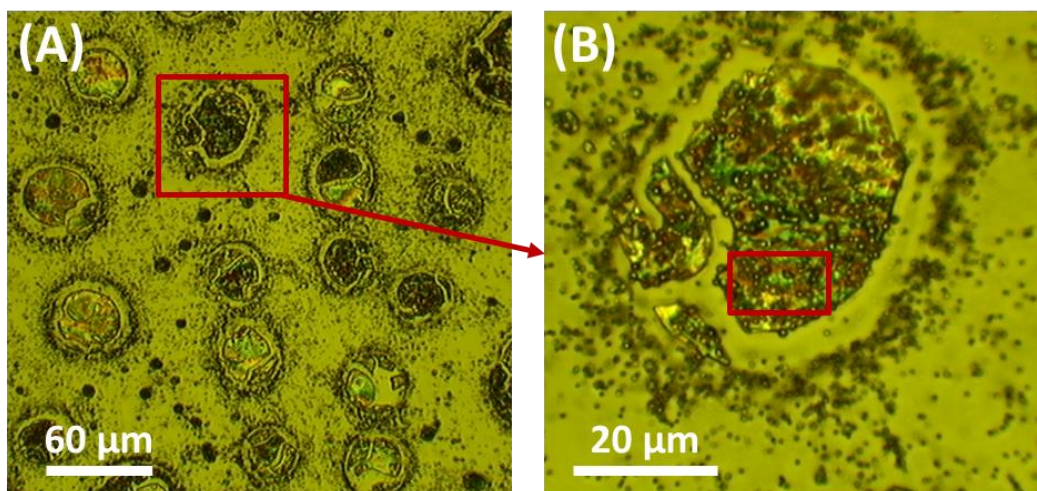

Figure S1. (A) and (B) optical micrographs of the sample prepared at 960 ºC discussed in Figure 1 of the main text. Figure S1B depicts the region marked with a red square on Figure S1A, showing the same region as the Scanning Electron Microscopy (SEM) image in Figure 1B of the main text. The red square in Figure B indicates the area that was mapped to obtain the Raman intensity image considered in Figure 1C of the main text.

Effect of Cetyl trimethylammonium bromide (CTAB) addition

CTAB is a capping-agent widely employed in the sol-gel method, its incorporation causes more aggregation of the nanostructures created.[1] The surface morphology of our samples may be attributed to CTAB addition since samples without this component do not exhibit such response, as shown in Figure S2.
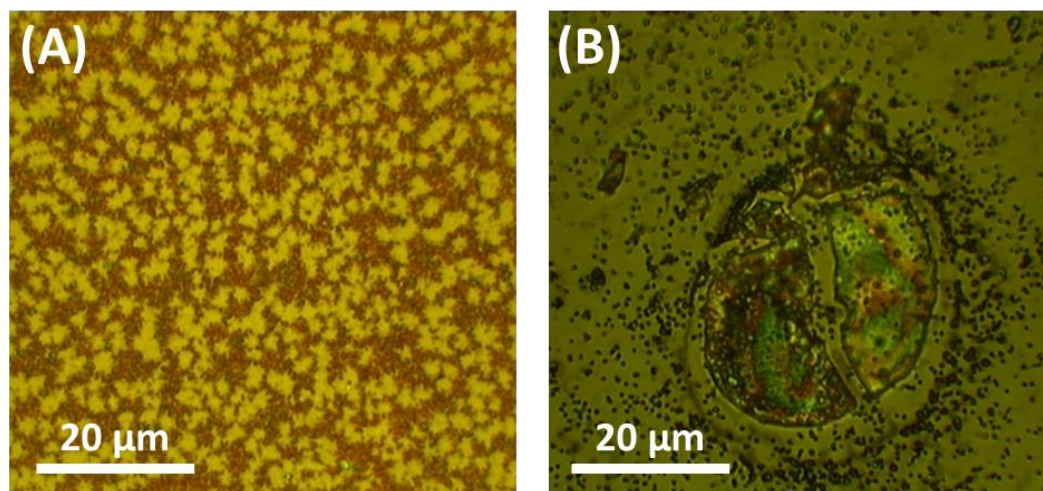

Figure S2. Optical micrographs of samples treated at 900 °C: (A) without and (B) with CTAB addition.

Particle size distribution for both thin film and powder samples

Particle size distribution associated with both powder form and grown on Si(100) substrates are depicted in Figure S3. The dimensions of these particles are obtained from Transmission Electron Microscopy (TEM) (powder samples) and SEM (thin film samples), using the ImageJ software. The diameter of the nanoparticles found in the powder samples are comprised between 4 nm and 35 nm, and the particle size distribution is fitted as a normal distribution with an average size of $\sim$ 16 nm. In contrast, the size of the micro- and nanoparticles synthesized on Si(100) substrates, ranges from 200 nm to 2.2 μm and the particle size distribution follows a log-normal distribution with an average particle size of 0.747 μm and FWHM of 0.707 μm.
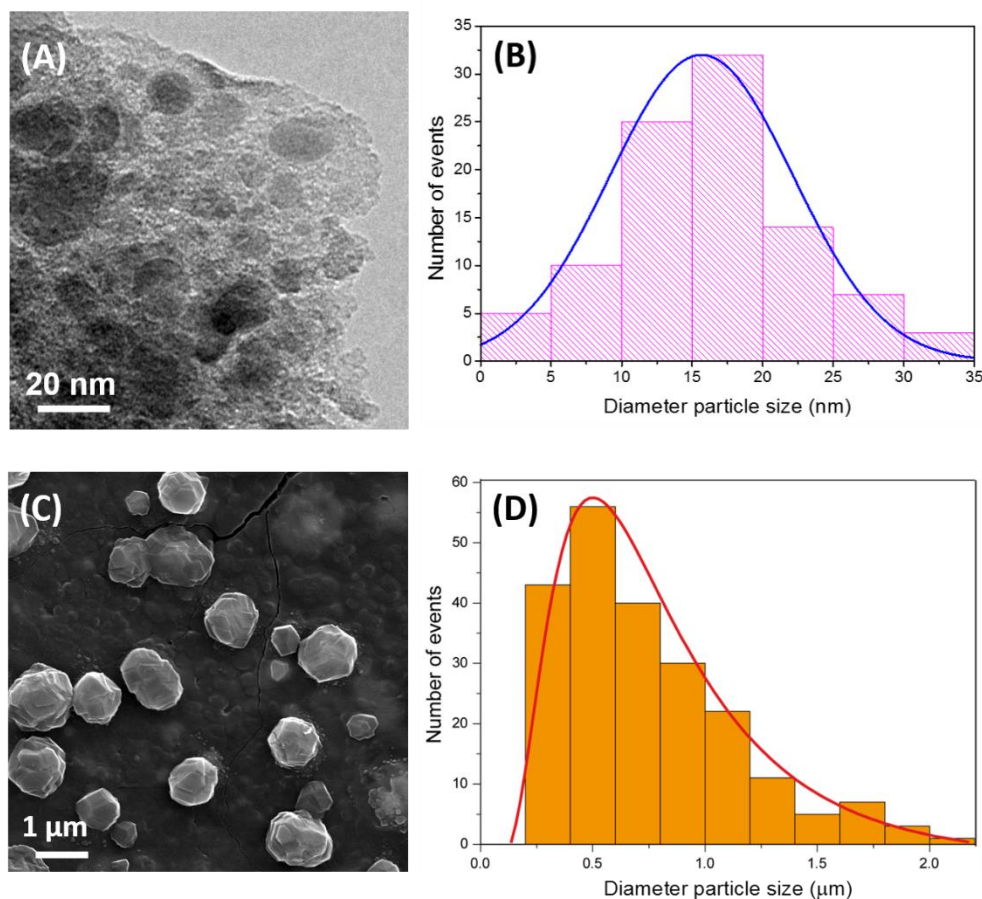

Figure S3. (A) TEM image and (B) particle size distribution of Fe_2O_3 nanoparticles in powder form. (C) SEM image and (D) particle size distribution of Fe_2O_3 particles grown on Si(100) substrates.

Raman spectrum for an ε-Fe₂O₃ microparticle measured with a 1800-g/mm grating

The Raman signal for an ε-Fe_2O_3 microparticle was also measured using an 1800-g/mm grating. Figure S4 shows the Raman spectrum taken at 100 K, which was obtained from an average of 5 spectra integrating 30 s each spectrum. We can observe a greater number of resolved Raman modes than using 600-g/mm grating (Figure 1D of the main text). In this measurement, we identify 52 vibrational modes between 100 and 850 cm^{-1}. Table S1 shows the wavenumbers obtained from a Lorentzian fitting of Raman spectrum bands.
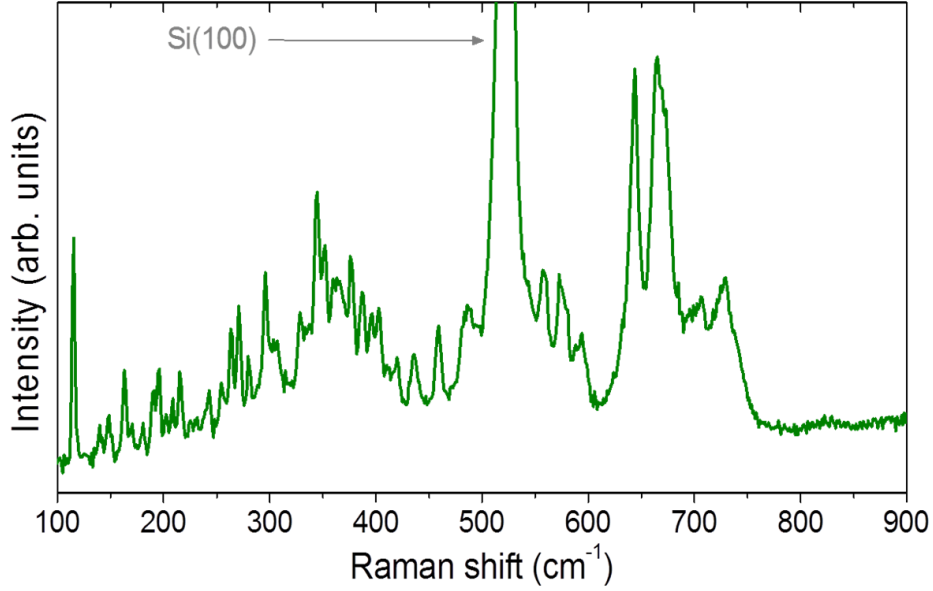

Figure S4. Raman spectrum measured at 100 K and obtained from an average of 5 spectra integrating 30 s each spectrum, using an 1800-g/mm grating. It is possible to distinguish 52 vibrational modes related to an ε-Fe_2O_3 microparticle ranging from 100 to 900 cm^{-1}.

Table S1. Raman modes and wavenumbers for ε-Fe$_2$O$_3$ Raman spectrum taken with an 1800-g/mm grating at 100 K.

ε-Fe$_2$O$_3$ (1800-g/mm grating)

Raman modes	Wavenumber (cm^{-1})	Raman modes	Wavenumber (cm^{-1})
B1	115.06 ± 0.04	B27	307.36 ± 0.45
B2	127.07 ± 0.96	B28	329.16 ± 0.15
B3	134.82 ± 2.34	B29	344.35 ± 0.07
B4	139.76 ± 1.98	B30	352.14 ± 0.12
B5	142.27 ± 3.02	B31	359.34 ± 0.25
B6	148.24 ±0.10	B32	365.90 ± 0.62
B7	151.94 ± 0.16	B33	376.63 ± 0.19
B8	163.21 ± 0.05	B34	386.98 ± 0.12
B9	170.17 ± 0.12	B35	395.21 ± 0.23
B10	178.58 ± 0.98	B36	403.09 ± 0.17
B11	181.09 ± 1.47	B37	419.95 ± 0.45
B12	190.04 ± 0.15	B38	436.10 ± 0.19
B13	195.63 ± 0.09	B39	458.96 ± 0.10
B14	202.23 ± 0.21	B40	486.83 ± 0.25
B15	208.38 ± 0.11	B41	557.67 ± 0.27
B16	215.56 ± 0.05	B42	574.23 ± 0.41
B17	225.38 ± 0.18	B43	580.60 ± 0.33
B18	228.84 ± 3.25	B44	593.18 ± 0.63
B19	231.73 ± 2.39	B45	598.09 ± 3.94
B20	243.02 ± 1.12	B46	643.65 ± 0.08
B21	254.72 ± 0.33	B47	663.99 ± 0.21
B22	263.68 ± 0.12	B48	672.97 ± 0.33
B23	270.88 ± 0.10	B49	704.92 ± 0.69
B24	280.22 ± 0.20	B50	728.22 ± 0.46
B25	295.86 ± 0.08	B51	741.42 ± 1.75
B26	303.23 ± 1.01	B52	823.40 ± 1.48

Laser light polarization dependence on ε-Fe₂O₃ Raman spectrum

Raman measurements changing the polarization of the incident laser light from 0° to 90° were performed on a single ε-Fe$_2$O$_3$ microparticle (marked with a white cross on Figure 1C), as shown in Figure S5. There are not significance differences, as can be checked in the SEM images in Figures 1A and 1B from the main text. However, slight intensity variations in some Raman bands have been observed, specially comparing to M2/M3, M9/M12 and M28/M29. Likely, this effect might be due to the faceted aspect of particles.
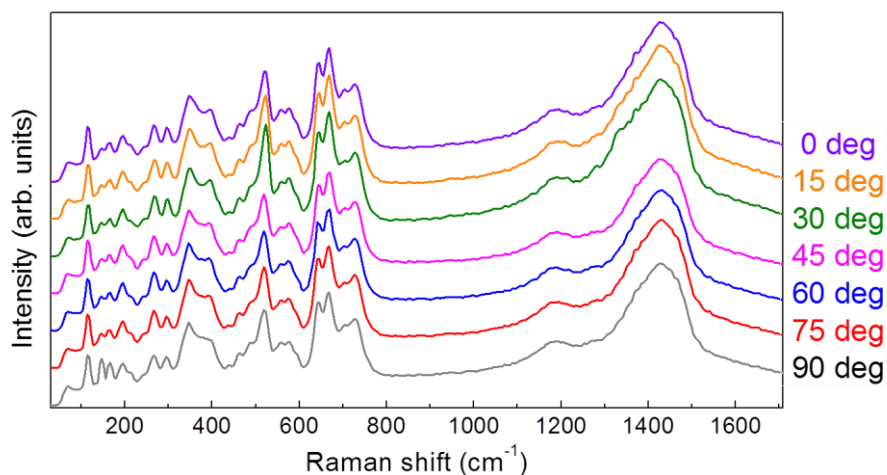

Figure S5. Average Raman spectra of 6 spectra integrating 10 s each spectrum of a ε-Fe$_2$O$_3$ particle marked with a white cross on Figure 1C of the main text, changing the polarization of the laser excitation from 0° to 90°.

Temperature dependence of ε-Fe₂O₃ nanoparticle agglomerates embedded in SiO₂ sol-gel films

In order to obtain $\varepsilon\text{-Fe}_2\text{O}_3$ microparticles we kept the temperature at 960 °C for 30 minutes. The nanoparticle agglomerates were grown in the same conditions as the microparticles, except for the stage at 960 °C for 30 minutes. In Figure S6B, the Atomic Force Microscopy (AFM) image shows particle agglomerates with a size of hundreds of nanometers, approximately. Besides, Figure S6C illustrates an in-plane Raman intensity image obtained from mapping the yellow region marked in Figure S6B. The ε-Fe₂O₃ nanoparticle agglomerate whose thermal evolution has been studied is marked with a yellow cross in AFM and Raman images (see Figures S6B and S6C). In this analysis, the tendency of the Raman spectrum as a function of temperature from 80 to 570 K was investigated (Figure S6A). Changes of Raman signal in the band position, intensity and linewidth were clearly observed. Raman bands are shifted towards larger wavenumbers and their intensity increases as temperature decreases. The resolution of ε-Fe₂O₃ Raman spectrum is gradually enhanced for lower temperatures. The Raman mode behavior for the nanoparticle agglomerate is qualitatively similar than for single microparticles.
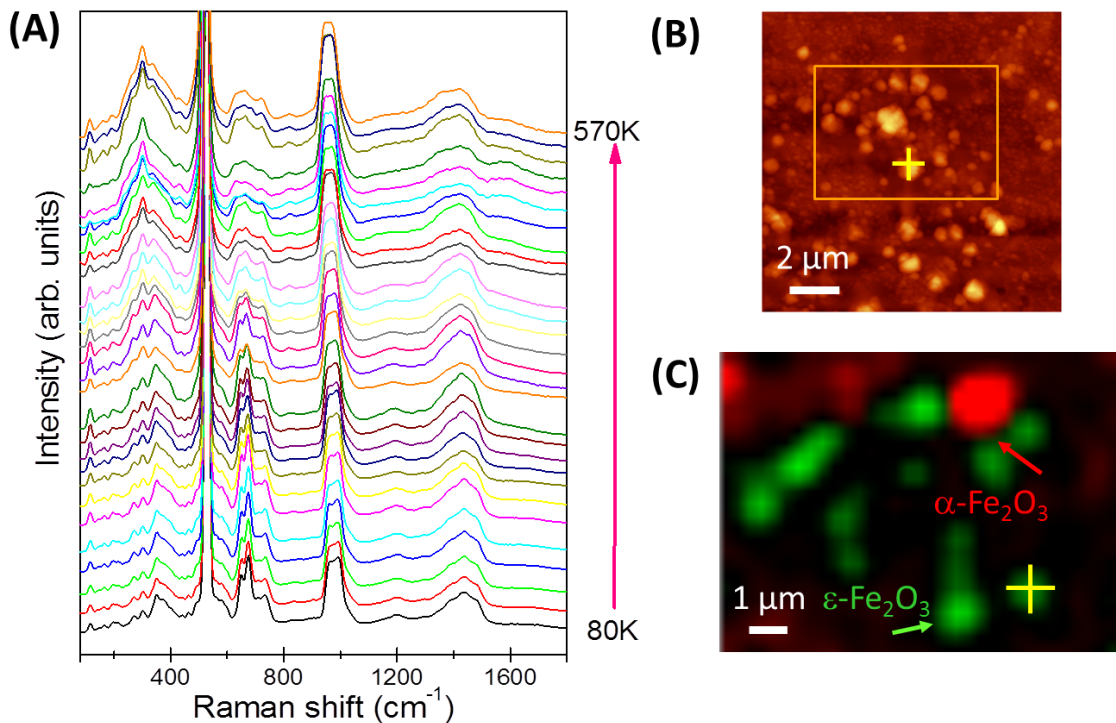

Figure S6. (A) Evolution of the Raman spectra as temperature increases from 80 to 570 K, (B) AFM image and (C) in-plane Raman intensity image obtained from the mapping of the region marked with a yellow square in Figure B, of a sample prepared at 960 °C. The yellow cross on Figures B-C marks the $\varepsilon\text{-Fe}_2\text{O}_3$ nanoparticle agglomerate studied in this experiment. Spectral range from 1200 to 1376 cm⁻¹ for α-Fe₂O₃ particles (in red) and from 1400 to 1576 cm⁻¹ for ε-Fe₂O₃ particles (in green) were integrated to obtain the Raman intensity image.

Further analysis was performed studying the behavior of the Raman bands as a function of temperature. Figure S7 presents the Raman shift and bandwidth for M1, M20 and M21 modes as a function of temperature for the ε-Fe₂O₃ nanoparticle agglomerate, respectively (see Figure S6B and S6C). Changes of Raman bands may vary depending on different phonon modes[2] and one consequence that can be deduced from the fittings is the possibility to observe some kind of phase magnetic transition.[3] Here, it is also notable the anomolous response across the Néel transition for ε-Fe₂O₃ particles.

Attending to the results for lower temperatures, we can infer that the resolution of ε-Fe₂O₃ Raman spectra is gradually enhanced, as expected. Moreover, subtle changes are detected in the bandwidth and Raman band shift for the M1, M20 and M21 modes ~ 130 K. These changes in the slope of the curves might be

originated by a structural transition. However, we have not observed a big enhancement of the relative intensities corresponding to the vibrational modes (as it happens across the Néel transition). We have neither observed the arising of new possible modes as a consequence of these slight distortions of the Fe^{3+} described above. With the present data, we can suggest a plausible magnetic transition around 130 K, which is more evidenced for the M1 mode. But the observations are not clear enough to unambiguously support the existence of a magnetic transition at low temperature.

Below 100 K, this material undergoes a magnetic transition from a collinear ferromagnetic state to a square-wave incommensurate magnetic structure. This transition is regarded as a second order structural transition involving subtle structural changes in the coordination of the Fe octahedral sites and Fe tetrahedral sites, occurring simultaneously as a result of the emergence of the incommensurate magnetic order.[4]

This experiment was also carried out on the epsilon microparticles and the results obtained are similar.
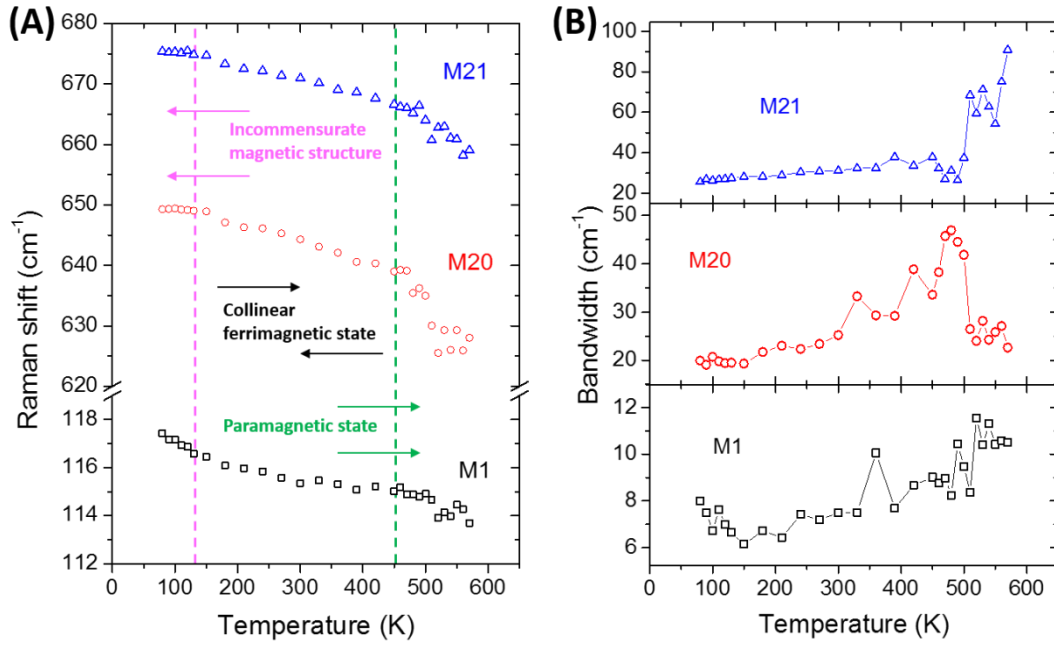

Figure S7. (A) Raman shift and (B) bandwidth evolution with temperature of M1, M20 and M21 for an ε-Fe$_2$O$_3$ nanoparticle agglomerate corresponding to the sample prepared at 960 °C.

Temperature dependence of a α-Fe$_2$O$_3$ single microparticle on SiO$_2$ sol-gel films

Figure S8A displays the behavior of the Raman spectrum of a single hematite particle as the temperature increases (marked with a yellow cross in Figure 1C in the manuscript)). Softening and red-shifts are observed in each vibrational Raman band with increasing temperature from 80 to 600 K, as found in the bibliography.[5,6] If we represent the relative Raman frequency as a function of temperature, we detect a drastic change in the tendency of the curve close to the Morin transition (which takes place around 260 K). Therefore, with Raman spectroscopy, we are able not only to observe a Néel transition as we have studied in this work for the epsilon phase, but also subtler magnetic transitions. Hematite undergoes, at the Morin transition, a change from an uncompensated or canted antiferromagnetic state to a perfectly compensated state as the temperature decreases.[7]
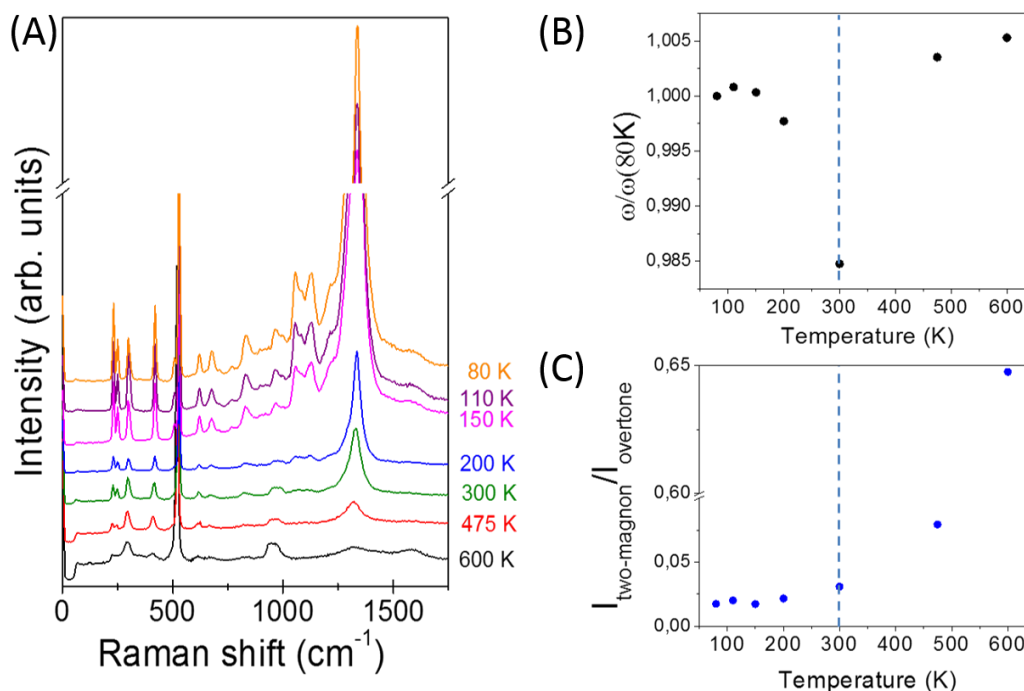

Figure S8. (A) Evolution of the Raman spectra from 80 K to 600 K of an α-Fe$_2$O$_3$ microparticle. (b) Evolution of ω(T)/ω(80 K) and (c) I$_{two-magnon}$/I$_{overtone}$ of the two-magnon mode in the α-Fe$_2$O$_3$ phase as a function of temperature.

References

(1) Wang, Z.; Li, X.; Feng, Z. Giant Coercive Field of Nanometer-Sized Iron Oxide. *Bull. Korean Chem. Soc.* **2011**, *32*, 1310–1314.

(2) Sahoo, S.; Gaur, A. P. S.; Ahmadi, M.; Guinel, M. J. F.; Katiyar, R. S. Temperature-Dependent Raman Studies and Thermal Conductivity of Few-Layer MoS$_2$. *J. Phys. Chem. C* **2013**, *117*, 9042–9047.

(3) Dubey, A.; Sathe, V. G. The Effect of Magnetic Order and Thickness in the Raman Spectra of Oriented Thin Films of LaMnO$_3$. *J. Phys. Condens. Matter* **2007**, *19*, 346232.

(4) Gich, M.; Frontera, C.; Roig, A.; Taboada, E.; Molins, E.; Rechenberg, H. R.; Ardisson, J. D.; Macedo, W. A. A.; Ritter, C.; Hardy, V.; Sort, J.; Skumryev, V.; Nogués, J. High- and Low-Temperature Crystal and Magnetic Structures of ε-Fe$_2$O$_3$ and Their Correlation to Its Magnetic Properties. *Chem. Mater.* **2006**, *18*, 3889–3897.

(5) Bertheville, B.; Bill, H.; Hagemann, H. Experimental Raman Scattering Investigation of Phonon Anharmonicity Effects in Li$_2$S. *J. Phys. Condens. Matter* **1999**, *10*, 2155–2169.

(6) Hajiyev, P.; Cong, C.; Qiu, C.; Yu, T. Contrast and Raman Spectroscopy Study of Single- and Few-layered Charge Density Wave Material: 2H-TaSe$_2$. *Sci.Rep.* **2013**, *3*, 2593.

(7) MacHala, L.; Tuček, J.; Zbořil, R. Polymorphous Transformations of Nanometric Iron(III) Oxide: A Review. *Chem. Mater.* **2011**, *23*, 3255–3272.